Mixed-valence hydrated iron fluoridotitanate: Synthesis, optics and calorimetry

Svetlana V. Mel'nikova [a], Natalia M. Laptash [b], Mikhail V. Gorev [a,c], Evgeniy I. Pogoreltsev [a,c,*]

[a] Kirensky Institute of Physics, Federal Research Center KSC SB RAS, 660036, Krasnoyarsk, Russia
[b] Institute of Chemistry, Far Eastern Branch of RAS, 690022, Vladivostok, Russia
[c] Siberian Federal University, 660074, Krasnoyarsk, Russia

ARTICLE INFO

ABSTRACT

Mixed-valence hydrated fluoridotitanate with idealized formula $FeTiF_6 \cdot 6H_2O$ is the main product of fluoride processing of natural mineral ilmenite with hydrofluoric acid. Its single crystals were grown and optical and calorimetric experiments were carried out in the temperature range 200–350 K. Charge re-distribution, $Fe^{2+}Ti^{4+}$ to $Fe^{3+}Ti^{3+}$, in the compound studied was evident in XPS spectra. A first order ferroelastic phase transition occurs at temperatures $T_{0\downarrow} = 271.5$ K, $T_{0\uparrow} = 274 \div 275.5$ K with the symmetry change $P\overline{3} \leftrightarrow P\overline{1}$. The structural transformation is accompanied by the appearance of a very weak optical anisotropy in the slice (001), a small anomaly of the heat capacity ($\Delta S = 1.5$ J/mol K $= 0.2R$), and positive baric coefficients $dT_0/dp \approx 30 \pm 10$ K/GPa.

1. Introduction

Iron and titanium are the most abundant elements in the Earth's crust (fourth and ninth places, respectively). Among transition metals, they are the first and the second most abundant in the geosphere. Both metals form the basis of the natural raw material ilmenite with the idealized formula $FeTiO_3$, which is highly available all around the world. It is the most abundant and economically important mineral as the chief source of titanium dioxide, TiO_2, which is used in paint pigments and in the manufacture of the metal titanium [1]. At the same time, methods to convert ilmenite into nanostructures of TiO_2 (which are required for new advanced applications, such as solar cells, batteries, and photocatalysts) have not been explored to any significant extent. The large-scale synthesis of TiO_2 nanostructures from cheap and abundant precursors is crucial for the transfer of dye-sensitized solar cells, new batteries with incorporated titania anodes, and efficient photocatalysts from the laboratory to "real life" applications [2].

Current industrial routes for the preparation of TiO_2 use either the sulfate or chloride processes, which still have faced a major problem to obtain white pigment of high purity and lower operation cost. The recovery of titanium dioxide from ilmenite ores by direct leaching technologies with the effect of several factors on the acid leaching kinetics was recently reviewed [3]. No use of hydrofluoric acid has been

considered. However, preliminary experiments on the dissolution of titanium and iron from ilmenite sand in various inorganic acids indicate that only hydrofluoric acid (HF) is the most effective [4–6]. It is a commercially available reagent, the generalized fluorination reaction of which with ilmenite (with the participation of atmospheric oxygen) was expressed in Ref. [5] as:

$$2FeTiO_3 + 14\ HF + 0.5O_2 = 2TiF_4 + 2FeF_3 + 7H_2O. \quad (1)$$

The other chemical fluorination reaction was presented by the following possible equation:

$$6HF + FeTiO_3 = Fe^{2+} + Ti^{4+} + 6F^- + 3H_2O. \quad (2)$$
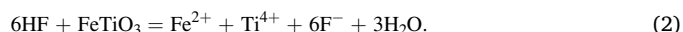
According to this relation, a ton of ilmenite concentrate would require about 0.8 tons HF for complete dissolution [7].

FeF_2 and TiF_4 form "double salt" $FeTiF_6 \cdot 6H_2O$ during the cooling of fluoride solutions being produced by dissolution of ilmenite in hydrofluoric acid [8]. The complex composition $FeTiF_6 \cdot 6H_2O$ was reported, for which only X-ray powder diffraction data were given. It was assumed that the crystal at ambient temperature has a symmetry $R\overline{3}m$ (166) with lattice parameters $a = b = 0.980$ nm, $c = 0.988$ nm, $Z = 3$ [9]. This compound belongs to the family $ABF_6 \cdot 6H_2O$ (A = Ni, Co, Zn, Mg, Mn, Fe, Cd; B = Ti, Si, Ge, Sn, Zr), in which the divalent atom (A) is surrounded by six water molecules and the tetravalent metal (B) is

---

surrounded by six fluorine atoms, forming almost regular octahedra additionally linked by 12 O–H$\cdots$F hydrogen bonds per chemical unit. These octahedra are packed in a rhombohedraly distorted CsCl-type structure. Many crystals of this family are known to undergo first order structural phase transitions (PTs). Investigations of twinning, birefringence, heat capacity and effect both of deuteration and of hydrostatic pressure (p) were carried out on those crystals. A generalized (p – T) phase diagram describing a variety of the phases observed in crystals of this family has been proposed [10,11]. Nevertheless, in spite of a lot of experimental results it was impossible to find the definite interrelations between the structure and phase transformations in these compounds.

Among the hexahydrated metal fluoridotitanates, the crystal structure was determined for the Zn- and Mn-salts [12] as well as for the Ni-salt [13]. All of them crystallize in space group $R\overline{3}$ at room temperature and are found to be ordered. Subsequent refinement of the $ZnTiF_6 \cdot 6H_2O$ structure showed, however, that they are actually disordered [14]. Crystal structure of $FeTiF_6 \cdot 6H_2O$ has not yet been determined, and this is a difficult task due to the twin nature of the synthesized crystals. Therefore, optical, dilatometric and calorimetric studies of the complex were initially carried out, which are presented in this paper.

2. Experimental section

2.1. Synthesis and composition

Usually, natural ilmenite contains some Fe(III) and appreciable quantities of magnesium and manganese. We were dealing with the approximate composition of $0.8FeTiO_3 \cdot 0.1Fe_2O_3$. Its interaction with hydrofluoric acid (40% weight) was highly exothermic. When the solution was cooled, red crystals of $Fe_2F_5 \cdot 7H_2O$ [15] first precipitated, and then long prisms (up to 20 mm elongated along the crystallographic *c* axis) of fluoridotitanate crystallized. However, the crystals were twins including the mother liquor and unsuitable for determining the structure. The same concerns the product of interaction of fluorotitanic acid with FeF_2 (from iron and concentrated HF). To grow more perfect crystals of the complex we used reagent grade chemicals, $TiCl_3$ or $Ti_2(SO_4)_3$-solutions (15% weight), $FeSO_4 \cdot 7H_2O$, and HF (40% weight). For example, 100 ml of $TiCl_3$ or $Ti_2(SO_4)_3$ with addition of 4–5 ml H_2O_2 (30% weight) and 35 ml of hydrofluoric acid were heated in a Pt beaker for 10–15 min, then 28 g of $FeSO_4 \cdot 7H_2O$ were added, and good yellowish-green prismatic single crystals were grown by slow evaporation of the solution in air at room temperature (Fig. 1). Their chemical analysis revealed the formula $Fe_{0.9}Ti_{1.1}F_6 \cdot 5.8H_2O$. Iron and titanium were determined by atomic absorption after the simple sample dissolution in distilled water, the reduced Fe^{2+} and Ti^{3+} were estimated by permanganate titration. Fluorine was analyzed by pyrohydrolysis at 400 °C and followed by titration with $Th(NO_3)_4$. EDX analysis confirmed the metal (Fe:Ti) ratio of 0.9:1.1. The powder XRD data of our compound is consistent in principle with that of Davidovich et al. [9] (PDF-2 card for $FeTiF_6 \cdot 6H_2O$ No. 00-025-0416) with addition of several minor lines and is provided in Supporting Information (Table S1).

X-ray photoelectron spectra (XPS) measurements of Fe(2p) and Ti (2p) electron spectra of iron fluoridotitanate were made with MgKα radiation at room temperature with residual pressure in the chamber of the energy analyzer of 5.10^{-8} Torr. Resolution for $4f_{7/2}$ gold peak was 1.4 eV. The XPS data (Fig. 2) indicate a mixed valence of transition metals in the investigated compound. The Ti 2p core-level photoelectron spectrum consists of two doublets. It is clear that the more intensive doublet with binging energies 462.4 and 468.0 eV is assigned to the Ti^{4+} sites in fluorine octahedron, while two distinct peaks of 460.5 and 466.3 eV correspond to the Ti^{3+} state. The two distinct peaks of 711.8 and 725.6 eV clearly indicate Fe^{2+} while the doublet of Fe^{3+} falls into the satellite region and can be associated, probably, with the binding
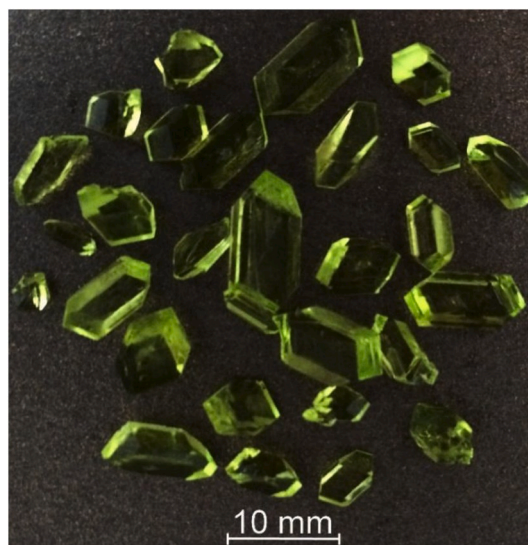
Fig. 1. Single crystals of $Fe_{0.9}Ti_{1.1}F_6 \cdot 5.8H_2O$.
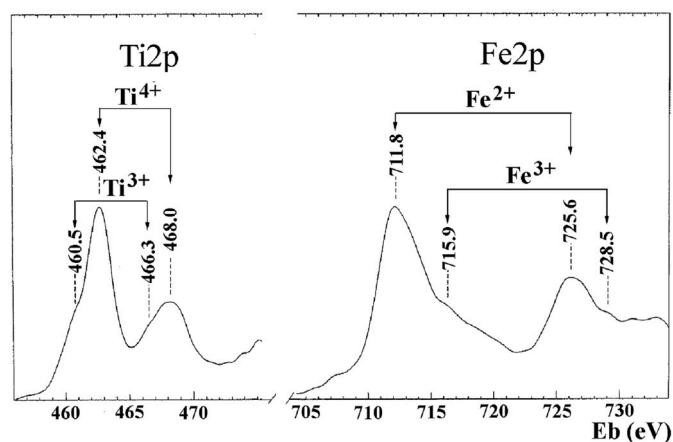
Fig. 2. XPS spectra of $Fe_{0.9}Ti_{1.1}F_6 \cdot 5.8H_2O$.

energies of 715.9 and 728.5 eV.

2.2. Characterisation methods

Optical studies were performed using a polarizing microscope Axioskop-40 and Linkam LTS 350 temperature chamber. The temperature investigations were carried out in a quasi-static mode with an accuracy of ±0.1 K in the range of 200–350 K. The extinction position and the angle of rotation of the indicatrix were determined with an accuracy of 0.5°. The birefringence was measured using a Berek compensator Leica with an accuracy of ≈0.00001.

Calorimetric measurements were performed on a differential scanning calorimeter NETZSCH 204 F1 (DSC). To study the heat capacity, a polycrystalline sample weighing ~20 mg was placed in an aluminum container (V = 25 mm³). Calorimetric studies were performed in the temperature range 220–310 K in a helium atmosphere (flow rate 20 ml/min) with a scan rate of 5 K/min.

Measurements of thermal expansion were performed using a pushrod dilatometer (NETZSCH model DIL-402C) with a fused silica sample holder. Experiments were carried out in the temperature range 100–300 K with a heating rate of 3 K/min in a dry He flux. In order to remove the influence of system thermal expansion, the results were calibrated by taking quartz as the standard reference. The reproducibility of the data obtained in successive series of the measurements was

not less than 5%. Samples for dilatometric measurements were prepared as quasi-ceramic disc-shaped pellets with a diameter of 6 mm and a thickness of ~1.5 mm.

3. Results

The grown large crystals have the shape of a hexagonal prism with (110) faces and [001] elongation. It should be noted that such a habit is characteristic for crystals with axial rhombohedral symmetry ($R\overline{3}$ or $P\overline{3}$), but not for planaxial ($R\overline{3}m$ or $P\overline{3}m$). Thus, we assume that the FeTiF$_6$·6H$_2$O (for simplicity, we will use the stoichiometric formula of the complex) crystal actually belongs to rhombohedral axial symmetry groups.

Polarization-optical studies and measurements of birefringence were carried out on oriented plates (001) and (100) in the temperature range 220–350 K. At ambient temperature the plate (001) is optically isotropic: it does not change the intensity of the passing polarized light when the microscope stage rotates. The direction [100] is located along the bisector of an obtuse angle (Fig. 3a). In the process of cooling, the isotropic state of the plate is continued to $T_{0\downarrow} = 271.5$ K (Fig. 3b), then the gray uniform pattern is broken, and bright extincting regions with small lamellar twins are formed, gradually filling total sample. To convert the entire sample at this temperature, a time interval of ~3 min is required.

The twin boundaries in the new phase are located both along [100] and along the slice of the hexagonal prism face [110] (Fig. 3c and d). Extinctions in different areas are rotated by an angle $\phi_c = \pm 9°$ relative to

these two directions and the angle value does not change with decreasing temperature. Upon repeated passes through the phase transition, the twin image does not repeat: the boundaries move, the regions expand, but the twinning laws remain the same. During heating, the transition to the optically isotropic state occurs through the formation and expansion of dark wedges of the high-temperature phase inside the anisotropic phase in the temperature range $T_{0\uparrow} = 274.5$–275.5 K (Fig. 3e).

The (100) plates have a precise extinction along [001] at room temperature, but below T_0 a banded twin pattern is visualized with colored uneven extinction due to the overlap of inclined twins (Fig. 3f). In the central region of the sample, where the twin boundaries are perpendicular to the surface of the sample, one can observe a good extinction, which differs from the initial one by a small angle $\phi_a = \pm 1.5°$.

The temperature behavior of the main birefringence Δn_a (T) = (n_o - n_e) (T) of the FeTiF$_6$·H$_2$O crystal is shown in Fig. 4. Curve 1 is obtained in the process of heating from low temperatures. At $T_{0\uparrow} = 274.5$ K, a weak anomaly is noticeable in the temperature dependence of the birefringence. Above 330 K, the surface of the sample becomes uneven, tuberous. The quality of the experiment deteriorates, and the measured values are significantly reduced. During the reverse course, the dependence Δn_a (T) (curve 2) does not repeat curve 1, but a weak anomaly is observed at $T_{0\downarrow} = 271.5$ K, revealing a temperature hysteresis $\delta T = 3$ K.

The processes of appearance and disappearance of the optical anisotropy in the (001) - plane are shown in Fig. 4 (curve 3). Birefringence from zero to a constant value $\Delta n_c = 0.0004$ appears upon cooling
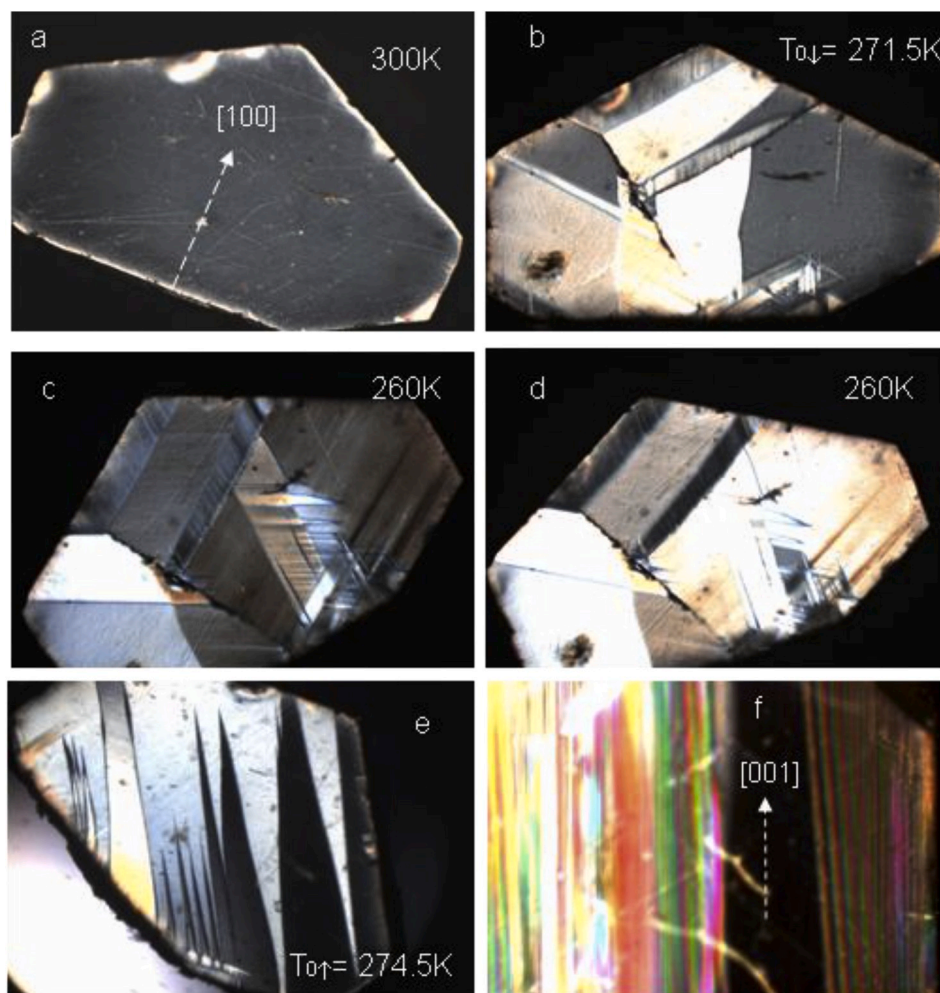
Fig. 3. Polarization-optical observations of various sections of the FeTiF$_6$·6H$_2$O crystal at different temperatures: (a − e) − (001) - cut; f − (100) - plate at T = 260 K.
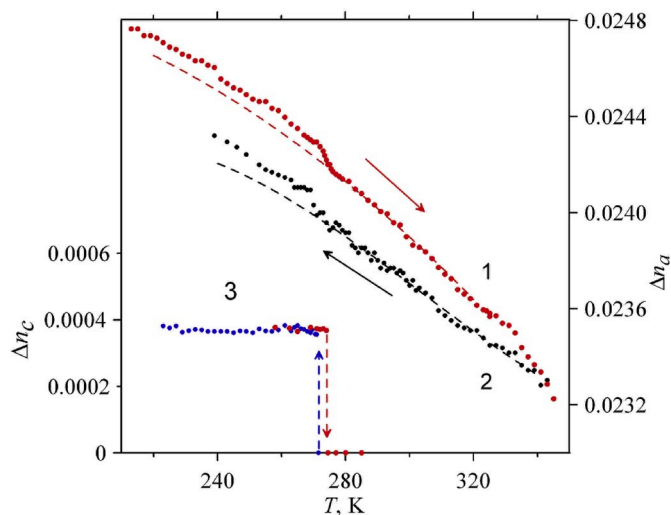
Fig. 4. Temperature dependences of birefringence in $FeTiF_6 \cdot 6H_2O$: $\Delta n_a(T)$ upon heating (1), upon cooling (2). Appearance and disappearance of Δn_c (T) in cooling-heating processes (3).

at $T_{0\downarrow} = 271.5$ K and disappears upon heating at $T_{0\uparrow} \approx 275$ K.

The measurements of the heat capacity, $C_p(T)$, of the $FeTiF_6 \cdot 6H_2O$ crystal were carried out over a temperature range $T = 220$–310 K. Fig. 5 shows the dependence of the DSC-signal on temperature in heating and cooling modes. The presence of an anomaly is clearly visible due to a reversible first-order phase transition. The transition temperature upon heating is $T_{0\uparrow} \approx 275.7$ K; upon cooling, the type of heat capacity anomaly is blurred and the transition temperature is more difficult to determine, but we suspect that it is $T_{0\downarrow} \approx 267$ K. The difference in DSC-anomalies during heating and cooling can be explained from the optical observations given above (made in a quasi-static mode). To complete the transition process upon heating ($T_{0\uparrow} = 274.5$–275.5 K), a temperature gradient is required, and upon cooling, a relaxation time $t \sim 3$–5 min is required. Therefore, the DSC anomaly during dynamic heating is sharper, and it is stretched along the temperature axis upon cooling. The enthalpy and entropy of the phase transition are $\Delta H \approx 423.5$ J/mol, and $\Delta S = \int (\Delta Cp/T) dT = 1.5$ J/mol·K, respectively.

Fig. 6 shows the results of the thermal dilatation measurements. The temperature behavior of the coefficient of volume thermal expansion, β, and volumetric strain, $\Delta V/V = 3\Delta L/L$, reveals.

Only one anomaly at $T_{0\uparrow} = 275.0 \pm 0.5$ K. The change in volume
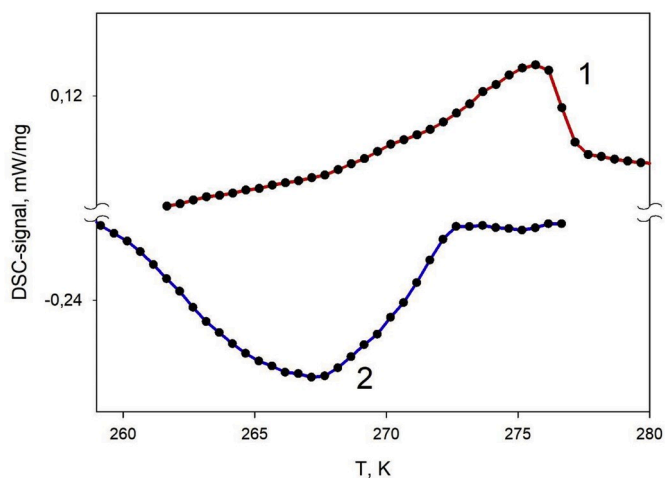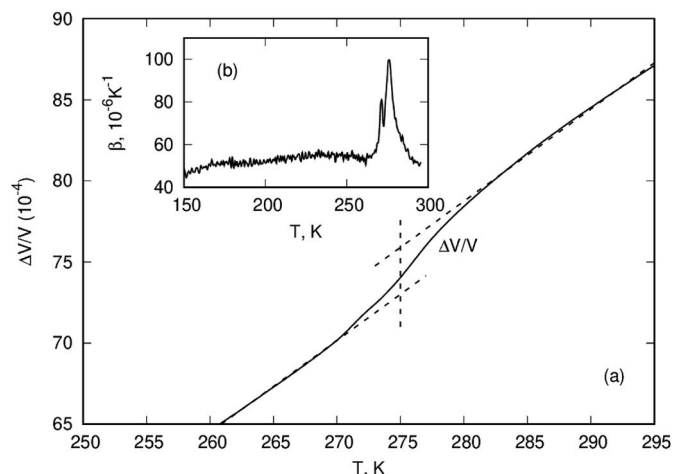
Fig. 6. Temperature dependencies of the volume strain $\Delta V/V$ (a) and thermal expansion coefficient β (b).

strain $\Delta V/V$ at T_0 equals approximately 89.9×10^{-6} and is positive. So, the baric coefficients dT_0/dp calculated using the Clausius-Clapeyron equation should be positive too $dT_0/dp = V_m(\Delta V/V)/\Delta S \approx 30 \pm 10$ K/GPa, where V_m is the molar volume and ΔS_0 and ΔV_0 are the jumps in entropy and volume at T_0, respectively.

4. Discussion

Interaction of natural mineral ilmenite with hydrofluoric acid proceeds exothermally with the formation of main product hydrated iron fluoridotitanate, the composition of which does not correspond the stoichiometric formula $FeTiF_6 \cdot 6H_2O$. In fact, it was $Fe_{0.9}Ti_{1.1}F_6 \cdot 5.8H_2O$. Charge re-distribution, $Fe^{2+}Ti^{4+}$ to $Fe^{3+}Ti^{3+}$, takes place in the studied compound similar to that in natural ilmenite. To understand the structural basis of the coordination environments around the Ti^{3+} would be very important, as these environments are one of the major factors that influence on the materials' electronic properties. And this is the task of the subsequent structural determination.

Belonging to the $ABF_6 \cdot 6H_2O$ family, the compound can be assigned to one of two groups. The first includes a phase transition of the $R\overline{3} \leftrightarrow P2_1/c$; for the second, information on the symmetry the high-temperature and low-temperature phases is ambiguous [10,11]. Our compound $FeTiF_6 \cdot 6H_2O$ belongs to the second group.

Conducted optical experiments show that a structural phase transition of the first order at $T_{0\downarrow} = 271.5$ K is observed in the crystal $FeTiF_6 \cdot 6H_2O$, which is accompanied by a change in the optical anisotropy, twinning and a decrease in the symmetry of compound. The rotation of the optical indicatrix around two axes (ϕ_a and ϕ_c) unambiguously indicates the triclinic symmetry of the low-temperature phase ($P\overline{1}$). The pseudo-rhombic cell of the low-temperature phase is aligned along [100], [110] and [001] of the initial rhombohedral phase. A similar twinning pattern was observed in the $MgTiF_6 \cdot 6H_2O$ crystal [16]: a large rotation of the optical indicatrix around the [001] axis ($\phi_c \approx 10°$) and weak rotation in the (100) plane ($\phi_a \approx 1°$). At present the data on the crystal structure of $MgTiF_6 \cdot 6H_2O$ are not available in the literature (no indication in Inorganic Crystal Structure Database, ICSD). However, the EPR study of $MgTiF_6 \cdot 6H_2O$ containing Mn^{2+} or Ni^{2+} proceeds from the existence of its low-temperature phase as monoclinic ($P2_1/c$) [17,18]. Really, according to X-ray diffraction data, the symmetry of the low-temperature phase for the related $FeSiF_6 \cdot 6H_2O$, $MnSiF_6 \cdot 6H_2O$, and $MgSiF_6 \cdot 6H_2O$ is monoclinic $P2_1/c$ [19–23]. Meanwhile, it was established by optical methods that their symmetry during phase transitions decreases to the triclinic $P\overline{1}$ [24,25]. The triclinic symmetry of the low-temperature phases of $FeSiF_6 \cdot 6H_2O$ and $MnSiF_6 \cdot 6H_2O$ is confirmed

Fig. 5. The temperature dependence of DSC-signal upon heating (1) and cooling (2).

by the results of a Raman scattering study in these crystals [26].

Despite the fact that, according to optical measurements and observations, a sharp first-order transition occurs in the crystal at T_0, its entropy is less than 0.2R. This may indicate slight structural changes during the phase transition and that the symmetry of the low-temperature phase is a subgroup of the initial one. Taking into account the habit of crystals in the form of a hexagonal prism, low transition entropy, weak birefringence anomalies, it can be argued with high probability that a structural phase transition $R(P)\overline{3} \leftrightarrow P\overline{1}$ occurs near the ice melting temperature. The fact that the twinning pattern does not repeat in different series of observations indicates the ferroelastic nature of the transition at T_0 in $FeTiF_6 \cdot 6H_2O$.

The choice between the two groups ($R\overline{3}$ or $P\overline{3}$) can be made based on the analysis of calorimetric experimental data [10,11,16], which shows that the thermodynamic characteristics are different for the two groups of crystals of the family $ABF_6 \cdot 6H_2O$. The entropy changes at phase transitions T_0 for crystals belonging to the first group is significantly larger ($\Delta S/R = 0.67$–0.95) (A-B: Co-Si, Co-Ti, Zn-Si, Zn-Ti, Mn-Ti) compared with the same value for the second ($\Delta S/R = 0.19$–0.38) (A-B: Fe-Si, Mg-Si, Mn-Si, Mg-Ti). For the latter case, it was found that the structural model of the high-temperature phase $R\overline{3}m$ given by Hamilton [27] should be replaced by $P\overline{3}$ [21,22,28,29], while the low-temperature phase is supposed to have the symmetry $P2_1/c$, which is not a subgroup of $P\overline{3}$. In addition, these two groups of crystals are distinguished by the signs of dT_0/dp.

The value of the transition entropy ($\Delta S/R \leq 0.2$) obtained in this work, the positive sign of the baric coefficient $dT/dp \approx 30$ K/GPa, and also the crystal habit allow us to choose $P\overline{3}$ as the symmetry group of the high-temperature phase of the $FeTiF_6 \cdot 6H_2O$ crystal, and the triclinic symmetry of the low-temperature phase $P\overline{1}$ is unambiguous from optical experiments. In confirmation, as follows from Raman studies of the related compounds $FeSiF_6 \cdot 6H_2O$ and $MnSiF_6 \cdot 6H_2O$, the number and symmetry of the observed lines are in good agreement with $P\overline{3}$ in the room-temperature phase and with the $P\overline{1}$ in the low-temperature phase [26].

The studies revealed the instability of the results of optical experiments at temperatures above 320 K, similar to those obtained previously on an $MgSiF_6 \cdot 6H_2O$ crystal [30,31]. The authors of these works associated this effect with the existence of an "incommensurate" phase in the crystal above 350 K. However, we see the reason for such instability in the loss of part of crystalline water near the surface of the sample and a decrease in its effective thickness. The same conclusion was made in Ref. [16], where the anomalies in the heat capacity and birefringence in $MgSiF_6 \cdot 6H_2O$ above 350 K were also explained by the evaporation of water.

5. Conclusions

In this study, we investigate $FeTiF_6 \cdot 6H_2O$, which is a fluorination product of the natural mineral ilmenite. Single crystals of good quality were obtained whose real composition corresponded to the formula $Fe_{0.9}Ti_{1.1}F_6 \cdot 5.8H_2O$. The presence of a mixed valence of transition metals (iron and titanium) is a characteristic feature of this compound. The complex belongs to the vast family of $ABF_6 \cdot 6H_2O$ compounds specifically to its second group, for which conflicting data are available in the literature on the structure of high- and low-temperature phases. The compound undergoes a first order ferroelastic phase transition at temperatures $T_{0\downarrow} = 271.5$ K, $T_{0\uparrow} = 274 \div 275.5$. The triclinic symmetry of the low-temperature phase $P\overline{1}$ is unambiguous from optical experiments. The value of the transition entropy ($\Delta S/R \leq 0.2$), the positive sign of the baric coefficient $dT/dp \approx 30$ K/GPa, as well as the crystal habit allow us to prefer $P\overline{3}$ as the symmetry group of the high-temperature phase.

Recently, unique properties of $ZnTiF_6 \cdot 6H_2O:Mn^{4+}$ red-emitting hexahydrate phosphor were described [32], unusual near-infrared

luminescence from Ti-doped $MgSiF_6 \cdot 6H_2O$ powder were observed [33], and the electrochemical synthesis of strongly luminescent $FeSiF_6 \cdot 6H_2O$ nano-powder from bulk metallurgical $FeSi_2/Si$ substrates was reported [34]. Various strategies are employed for enhancing the photocatalytic and photoelectrocatalytic performance of Ti-based and Fe-based materials. The most outstanding improvements in the activity can be obtained by the combination of hematite and TiO_2 [35]. We believe that the hydrated iron fluoridotitanate can serve as a precursor for the synthesis of such materials.

Declaration of competing interest

The authors declare that they have no known competing financial interests or personal relationships that could have appeared to influence the work reported in this paper.

CRediT authorship contribution statement

Svetlana V. Mel'nikova: Investigation, Writing - original draft, Conceptualization. **Natalia M. Laptash:** Investigation, Supervision, Writing - original draft, Writing - review & editing. **Mikhail V. Gorev:** Investigation. **Evgeniy I. Pogoreltsev:** Investigation, Writing - original draft, Writing - review & editing.

Appendix A. Supplementary data

Supplementary data to this article can be found online at https://doi.org/10.1016/j.jpcs.2020.109444.

References

[1] F. Habashi, Interdiscipl. J. Chem. 1 (1) (2016) 28–33.
[2] T. Tao, Y. Chen, D. Zhou, H.Z. Zhang, S. Liu, R. Amal, N. Sharma, A.M. Glushenkov, Chem. Eur J. 19 (2013) 1091–1096.
[3] T.H. Nguyen, M.S. Lee, Miner, Processing extr, Metall. Rev. 40 (4) (2018) 231–247.
[4] R.K. Biswas, M.G.K. Mondal, Hydrometallurgy 17 (1987) 385–390.
[5] D.A. Hansen, D.E. Traut, JOM – J. Miner. Metals Mater. Soc. 41 (5) (1989) 34–36.
[6] R.K. Biswas, M.A. Habib, N.C. Dafader, Hydrometallurgy 28 (1992) 119–126.
[7] M.M. Ali, K.F. Mahmoud, A.A. Dewedar, Minufiya Univ. Sci. J. Fac. Sci. 17 (2003) 309–331.
[8] N. Keisuke, Y. Hideyuki, H. Toshio, K. Takaho, EP 0319857 A1, Eur. Patent (1989). Publ. 14.06.89.
[9] R.L. Davidovich, T.A. Kaidalova, T.F. Levchishina, Zh. Strukt. Khim. 12 (1971) 185–187.
[10] I.N. Flerov, M.V. Gorev, S.V. Melnikova, M.L. Afanasyev, K.S. Aleksandrov, Ferroelectrics 143 (1993) 11–16.
[11] I.N. Flerov, M.V. Gorev, K.S. Aleksandrov, M.L. Afanasyev, J. Phys.: Condens. Mater. 4 (1992) 91–99.
[12] T. Chattopadhyay, F. Devreux, K. Peters, E.-M. Peters, E. Gmelin, B. Ghosh, J. Phys. C Solid State Phys. 21 (1988) 1321–1334.
[13] P. Halasyamani, M.J. Willis, C.L. Stern, K.R. Poeppelmeier, Inorg. Chim. Acta. 240 (1995) 109–115.
[14] G. Mostafa, S. Ray, A. Mukhopadhyay, Z. Kristallogr. 211 (1996) 373–377.
[15] U. Bentrup, Thermochim. Acta 284 (1996) 397–406.
[16] I.N. Flerov, M.V. Gorev, S.V. Melnikova, M.L. Afanasyev, K.S. Aleksandrov, Fiz. Tverd. Tela 33 (1991) 1921–1929.
[17] R.S. Rubins, Y.H. Yung, J. Chem. Phys. 75 (1981) 4285–4288.
[18] A.M. Ziatdinov, V.G. Kuryavyi, R.L. Davidivich, Fiz. Tverd. Tela 28 (1986) 3549–3551.
[19] E. Kodera, A. Torii, K. Osaki, T. Watanabe, J. Phys. Soc. Jap. 32 (1972) 863.
[20] G. Jehanno, F. Varret, Acta Crystallogr. A31 (1975) 857–858.
[21] G. Chevrier, G. Jehanno, Acta Crystallogr. A35 (1979) 912–916.
[22] G. Chevrier, A. Hardy, G. Jehanno, Acta Crystallogr. A37 (1981) 578–584.
[23] S. Syoyama, K. Osaki, Acta Crystallogr. B28 (1972) 2626–2627.
[24] V.V. Eremenko, A.V. Peschansky, V.I. Fomin, Kristallografiya 34 (1989) 658–662.
[25] V.P. Gnezdilov, V.V. Eremenko, A.V. Peschansky, V.I. Fomin, Fiz. Tverd. Tela 34 (1992) 232–237.
[26] V.V. Eremenko, A.V. Peschansky, V.I. Fomin, Fiz. Tverd. Tela 39 (1997) 929–939.
[27] W.C. Hamilton, Acta Crystallogr. 15 (1962) 353–360.
[28] G. Chevrier, J. Solid State Chem. 99 (1992) 276–282.

[29] A. Torii, K. Ogawa, H. Tamura, K. Osaki, Acta Crystallogr. C53 (1997) 833–836.

[30] R. Hrabanski, V. Kapustianik, V. Kardash, S. Sveleba, Phys. Status Solid. (A) 142 (1994) 509–514.

[31] P.G. Skrylnik, A.M. Ziatdinov, Appl. Magn. Reson. 45 (2014) 623–640.

[32] R. Hoshino, S. Sakurai, T. Nakamura, S. Adachi, J. Lumin. 184 (2017) 160–168.

[33] S. Sakurai, T. Nakamura, J. Lumin. 211 (2019) 157–161.

[34] A. Pastushenko, V. Lysenko, RSC Adv. 6 (2016) 8093–8095.

[35] Y. AlSalka, L.I. Granone, W. Ramadan, A. Hakki, Appl. Catal. B Environ. 244 (2019) 1065–1095.